JOURNAL OF SOLID STATE CHEMISTRY 79, 19–27 (1989)

A Raman Study of the Systems $Fe_{3-x}Cr_xO_4$ and $Fe_{2-x}Cr_xO_3$*

K. F. McCARTY AND D. R. BOEHME

Sandia National Laboratories, Livermore, California 94550

Received September 8, 1988

Raman spectra of the solid solutions $Fe_{3-x}Cr_xO_4$ ($0 \leq x \leq 2$) and $Fe_{2-x}Cr_xO_3$ ($0 \leq x \leq 2$) have been obtained. The fundamental, overtone, and combination vibrational bands observed are examined in terms of the variations occurring in the structures of the spinel-type ($Fe_{3-x}Cr_xO_4$) or corundum-type ($Fe_{2-x}Cr_xO_3$) solid solutions. For $Fe_{3-x}Cr_xO_4$, the Raman shift of the dominant feature at ~675 cm^{-1} varies inversely with the volume of the unit cell. Shoulders on the ~675 cm^{-1} peaks of $Fe_{1.4}Cr_{1.6}O_4$ and $Fe_{1.8}Cr_{1.2}O_4$ are believed to result from partial ordering of the cations in these materials. For $Fe_{2-x}Cr_xO_3$ containing both iron and chromium, a fundamental vibration not observed in either α-Fe_2O_3 or Cr_2O_3 is the dominant Raman-scattering feature.

Introduction

Solid solutions of iron and chromium oxides adopt either corundum or spinel structure (*1, 2*). These solid solutions occur naturally and are commonly formed during the oxidation of iron/chromium alloys (*3*). The cubic solid solution $Fe_{3-x}Cr_xO_4$ ($0 \leq x \leq 2$) with the spinel structure has Fe_3O_4 and $FeCr_2O_4$ as its limiting compositions. The structure consists of a cubic-close-packed oxygen lattice with cations at both the octahedral and tetrahedral interstices (*4*). $FeCr_2O_4$ is a normal spinel with Cr^{3+} ions occupying one-half of the octahedral coordination sites and with Fe^{2+} occupying one-eighth of the tetrahedral sites. Fe_3O_4 is an inverse spinel with half the Fe^{3+} ions in the tetrahedral sites and with the Fe^{2+} ions and the other half of the Fe^{3+} ions in the octahedral sites. The rhombohedral solid solution $Fe_{2-x}Cr_xO_3$ ($0 \leq x \leq 2$) with the corundrum structure has α-Fe_2O_3 and Cr_2O_3 as its limiting compositions. The structure consists of a hexagonal-close-packed oxygen lattice in which Fe^{3+} and Cr^{3+} ions together occupy two-thirds of the octahedral interstices (*4*).

In this paper, we report the Raman spectra of the spinel-structure solid solutions $Fe_{3-x}Cr_xO_4$ with $0 \leq x \leq 2$ and the corundum-structure solid solutions $Fe_{2-x}Cr_xO_3$ with $0 \leq x \leq 2$. The systematic variations occurring in the spectra are examined in terms of the structural variations occurring in the solid solutions. Additional Raman bands, features that are not found in the limiting compositions of the solid solutions, are found for a portion of the $Fe_{3-x}Cr_xO_4$ solid solution and for the entire $Fe_{2-x}Cr_xO_3$ solid solution. These bands arise from structural distortions and/or cation orderings that are not observable by X-ray powder diffraction.

* This work was supported by the U.S. Department of Energy, Office of Basic Energy Sciences, Division of Material Sciences, under contract DEAC04-76DP00789.

0022-4596/89 $3.00

Experimental Procedure

The Fe_2O_3–Cr_2O_3 solid solutions were prepared by grinding α-Fe_2O_3 (Puratronic) and Cr_2O_3 (Puratronic) powders together in an agate mortar and pestle and pressing the mixtures into pellets. The pellets were placed in alumina crucibles and heated at 800°C for 6 hr in air. Following air quenching to room temperature, the pellets were crushed, ground, and repressed into pellets. After heating for 24 hr in air at 1200°C, the pellets were quenched to room temperature. A series of materials $Fe_{2-x}Cr_xO_3$ with x = 1.60, 1.33, 1.07, 0.80, 0.53, and 0.27 were prepared. In addition, samples of pure Cr_2O_3 and α-Fe_2O_3 were prepared by heating pellets of the pure powders at 800°C for 6 hr, followed by air quenching to room temperature. Spinel solid solutions, $Fe_{3-x}Cr_xO_4$, with x = 0, 0.4, 0.8, 1.2, and 2.0 were prepared by reducing the appropriate $Fe_{2-x}Cr_xO_3$ material. $Fe_{2-x}Cr_xO_3$ pellets were heated at 1300°C for 6 hr in alumina crucibles held inside an alumina tube through which either pure CO_2 or a 46% H_2/54% CO_2 mixture was flowed. The samples were quenched to room temperature by withdrawing the alumina tube from the furnace. At 1300°C, a pure CO_2 atmosphere produces an oxygen partial pressure of 3.7×10^{-4} atm, while a 46% H_2/54% CO_2 mixture produces an oxygen partial pressure of 1.0×10^{-10} atm (5). Spinel materials $Fe_{3-x}Cr_xO_4$ with x = 0, 0.4, 0.8, 1.2, and 1.6 were prepared in the CO_2 flow, while x = 1.6 and 2.0 were prepared in the H_2/CO_2 flow. An additional Fe_3O_4 sample was prepared by heating an α-Fe_2O_3 pellet at 1300°C for 6 hr in a vacuum of $\sim 5 \times 10^{-5}$ Torr, followed by furnace cooling to room temperature.

Raman spectra were obtained at room temperature in a backscattering arrangement from pellets spun at about 1000 rpm. The 514.5-nm argon-ion laser beam was incident normal to the surface of the pellets and scattered radiation was collected about the surface normal using a pierced mirror. Spectra were obtained using a Spex Triplemate spectrograph and an intensified diode-array detector. By centering the spectrograph at two different wavelengths, the spectral range of ~200 to 1000 cm^{-1} and ~1000 to 1600 cm^{-1} were examined. The laser power focused on the samples was 150 mW and spectra were collected in 250 sec, except for Cr_2O_3 and $FeCr_2O_4$ for which shorter times were used. A neon lamp was used to calibrate the spectrograph.

X-ray diffraction (XRD) was used to determine the phase purity and crystallographic lattice constants of each sample. All materials were found to be single phase. XRD analysis was performed using a Rigaku 18-kW rotating anode diffraction system equipped with a Cu-target anode. The powder samples were scanned from 100 to 140° 2θ using a 250° wide-angle goniometer equipped with a graphite monochromator. Alpha-quartz was used as an external calibration standard. Lattice parameters for each specimen were calculated by a least-squares refinement of all reflections in the range 100–140°. The error in the measured lattice constant resulting from sample positioning and instrument precision is estimated to be ±0.003 Å.

Results: $Fe_{3-x}Cr_xO_4$ Solid Solutions

The Raman spectra of the spinel-type solid solutions $Fe_{3-x}Cr_xO_4$ with x = 0.0, 0.4, 0.8, 1.2, 1.6, and 2.0 are shown in Fig. 1. The strongest feature of all the phases occurs at ~675 cm^{-1}. While this band is relatively sharp and symmetric for $FeCr_2O_4$, a shoulder appears on the low wavenumber side for $Fe_{1.4}Cr_{1.6}O_4$ (at ~636 cm^{-1}) and $Fe_{1.8}Cr_{1.2}O_4$ (at ~636 cm^{-1}). No shoulders are apparent for $Fe_{2.2}Cr_{0.8}O_4$, $Fe_{2.6}Cr_{0.4}O_4$, and Fe_3O_4. Peak positions and the full-width-at-half-maximum (FWHM) values for the ~675 cm^{-1} band are given in Table I.

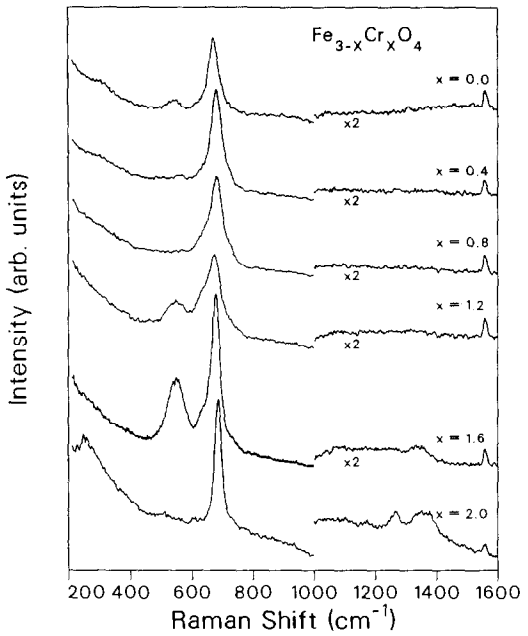

FIG. 1. Raman spectra of spinel-structure solid solution: $Fe_{3-x}Cr_xO_4$ with $x = 0.0, 0.4, 0.8, 1.2, 1.6$, and 2.0 using a 514.5-nm laser. Scale factors are shown. Peak at 1558 cm^{-1} is from atmosphere O_2.

The FWHM values range from 26 cm^{-1} for $FeCr_2O_4$ to 49 cm^{-1} for $Fe_{1.8}Cr_{1.2}O_4$. (No attempt was made to account for the shoulders of the $Fe_{1.8}Cr_{1.2}O_4$ and $Fe_{1.4}Cr_{1.6}O_4$ materials in the FWHM determinations.) The spectrum of magnetite, Fe_3O_4, has a weak band at 543 cm^{-1}. The substitution of Cr for Fe in the structure initially causes a reduction in the intensity of this band ($Fe_{2.6}Cr_{0.4}O_4$), and for $Fe_{2.2}Cr_{0.8}O_4$, the band is not discernable. However, with the introduction of more Cr, the band reappears ($Fe_{1.8}Cr_{1.2}O_4$), and for $Fe_{1.4}Cr_{1.6}O_4$, the band is relatively intense and extremely broad (FWHM = 53 cm^{-1} for $Fe_{1.4}Cr_{1.6}O_4$). Two materials exhibited Raman-scattering features at higher wavenumbers—$FeCr_2O_4$ has a peak at ~1265 cm^{-1} and a broader feature at ~1357 cm^{-1}. $Fe_{1.4}Cr_{1.6}O_4$ has a weak, broadband at ~1335 cm^{-1}. All spectra of Fig. 1 show a band at 1558 cm^{-1} resulting from the vibrational stretch of atmospheric O_2 (*6*).

Table I also contains the lengths of the cubic unit cells of $Fe_{3-x}Cr_xO_4$ as determined by XRD analysis. The variations of cell length with chromium content agree well with literature results and the absolute values are in reasonable agreement (*1, 7*). In the (room temperature) XRD spectra, there was no evidence of superlattice reflections, nor was there any evidence that the unit cells were distorted away from full cubic symmetry.

Raman spectra were also obtained from an Fe_3O_4 sample prepared by heating α-Fe_2O_3 in vacuum at 1300°C and an $Fe_{1.4}Cr_{1.6}O_4$ sample prepared by reducing $Fe_{0.93}Cr_{1.07}O_3$ in an H_2/CO flow. Both of these materials had Raman spectra very similar to their counterparts of Fig. 1 and Table I. Despite the differences in preparation conditions, the Raman shifts were practically identical. However, the 679 cm^{-1} band of the $Fe_{1.4}Cr_{1.6}O_4$ sample prepared in the H_2/CO environment was somewhat broader (37 cm^{-1}) than the band of the sample prepared in a pure CO_2 environment (31 cm^{-1}).

TABLE I

OBSERVED RAMAN BANDS AND CUBIC CELL LENGTHS FOR $Fe_{3-x}Cr_xO_4$

Fe_3O_4 a = 8.398 (1)	542	—	671 (38)	—	—
$Fe_{2.6}Cr_{0.4}O_4$ a = 8.396 (4)	562	—	682 (39)	—	—
$Fe_{2.2}Cr_{0.8}O_4$ a = 8.398 (1)	—	—	681 (44)	—	—
$Fe_{1.8}Cr_{1.2}O_4$ a = 8.408 (1)	548	636s	674 (49)	—	—
$Fe_{1.4}Cr_{1.6}O_4$ a = 8.398 (1)	550	636s	679 (31)	—	1335
$FeCr_2O_4$ a = 8.381 (1)	—	—	686 (26)	1265	1357

Note. All Raman shift values are in cm^{-1}. Values given in parentheses after ~675 cm^{-1} position are FWHM in cm^{-1}. s = shoulder. Cubic cell length a is in Å, with error of last digit in parentheses.

Discussion: $Fe_{3-x}Cr_xO_4$ Solid Solutions

A group-theory (factor group) analysis of the cubic spinel structure with space group $Fd3m$ (O_h^7) predicts five Raman-allowed, fundamental, vibrational modes (*8*). For Fe_3O_4, these modes have all been observed in single-crystal studies (*8*). On the basis of the Fe_3O_4 results, the ~675 and ~550 cm^{-1} Raman features of the entire $Fe_{3-x}Cr_xO_4$ solid solution can be assigned to A_{1g} and T_{2g} symmetries, respectively. The three weaker phonons, occurring at 420 cm^{-1} (T_{2g}), 320 cm^{-1} (E_g), and 298 cm^{-1} (T_{2g}) in Fe_3O_4, are not observed in the present study of polycrystalline materials.

In Table I, the Raman shift of the A_{1g} phonon is seen to be inversely related to the cubic cell length. That is, as the unit cell contracts (expands) the vibrational frequency increases (decreases). The Grüneisen constant for this mode,

$$\gamma = -\frac{d(\ln v)}{d(\ln V)},$$

with v being the Raman shift and V the volume of the unit cell, is 2.0, assuming a linear relationship between ln v and ln V. This reasonable value for the Grüneisen constant establishes that normal phonon behavior occurs in the solid solution (*9*).

The FWHM values of the 671 cm^{-1} mode (A_{1g}) of Fe_3O_4 is 38 cm^{-1} at room temperature, in good agreement with the results of Verble (*10*). Verble interpreted the large linewidth as arising from the electronic disorder in the structure. That is, the random distribution of Fe^{2+} and Fe^{3+} ions on equivalent B (octahedral) sites of the structure results in spatial fluctuations in the electron charge density. This argument is consistent with the smaller linewidths of $FeCr_2O_4$ and $Fe_{1.4}Cr_{1.6}O_4$ (Table I). The normal spinel $FeCr_2O_4$ has only Cr^{3+} on the B sites while $Fe_{1.4}Cr_{1.6}O_4$ has only trivalent Cr^{3+} and Fe^{3+} on the B sites (*11*). This implies, as suggested by Verble, that the "compositional" disorder resulting from the substitution of electronically similar elements (here Cr^{3+} and Fe^{3+}) causes less broadening than the "chemical" disorder resulting from having Fe^{2+} and Fe^{3+} on equivalent sites.

Two interesting effects occur when the composition changes from $FeCr_2O_4$ to $Fe_{1.4}Cr_{1.6}O_4$ and $Fe_{1.8}Cr_{1.2}O_4$. For these latter two materials, the A_{1g} phonon at ~675 cm^{-1} develops a prominent low wavenumber shoulder. In addition, the ~550 cm^{-1} feature becomes intense and extremely broad. For these same two materials, Gillot *et al.* (*12*) showed that the ν_3 IR band at ~370 cm^{-1} was split into a doublet. An explanation for the new features of $Fe_{1.4}Cr_{1.6}O_4$ and $Fe_{1.8}Cr_{1.2}O_4$ would be that these phases do not have the $Fd3m$ structure of the parent spinel. For example, the presence of a superlattice would allow additional Raman modes through the introduction of a larger unit cell with additional degrees of freedom. A distortion to a lattice of lower symmetry allow additional Raman bands by lifting of degeneracies or allowing modes that are inactive in the parent structure to become active. However, on the basis of the XRD analyses in this study and others (*1*) for $Fe_{3-x}Cr_xO_4$ at room temperature, there is no indication of either superlattices or distortions to lattices of lower symmetry. (However, upon cooling below room temperature, Levinstein *et al.* (*1*) observed lattice distortions for certain compositions. $Fe_{1.8}Cr_{1.2}O_4$ is on the border between compositions for which no low temperature distortion occurs ($0 \leq x \leq 1.2$) and compositions for which a cubic–tetragonal transition occurs ($1.25 \leq x \leq 1.32$). $Fe_{1.4}Cr_{1.6}O_4$ is in the composition region ($1.4 \leq x \leq 1.7$) for which cubic–tetragonal–orthorhombic transitions occur. For $1.7 \leq x \leq 2$, a cubic-to-orthorhombic transition occurs. Thus, the additional Raman features are associated with the materials which undergo a low temperature cubic/tetragonal distortion.)

Since there is no evidence that the additional Raman features of $Fe_{1.4}Cr_{1.6}O_4$ and $Fe_{1.8}Cr_{1.2}O_4$ result from structural distortions, it is suggested that they arise from a partial ordering of the cations. DeAngelis *et al.* (*13*) and Keramidas *et al.* (*14*) investigated spinels with various types of cation ordering on the octahedral and tetrahedral sites. In general, completely ordered spinels exhibit a larger number of Raman and IR bands than the parent disordered material. Kermidas *et al.* (*14*) provide the example of the ordered and "disordered" form of the spinel $LiGaTiO_4$. The ordered, orthorhombic material exhibits a Raman spectrum consisting of at least 20 bands, while the Raman spectra of "disordered" $LiGaTiO_4$ has the expected 5 Raman bands, several of these possessing significant shoulders. The authors felt that the shoulders arose from partial ordering of the cations. The similarity between the results of $LiGaTiO_4$ and $Fe_{1.4}Cr_{1.6}O_4$ and $Fe_{1.8}Cr_{1.2}O_4$ suggests that partial ordering of the cations also occur in the latter two materials. In $Fe_{1.4}Cr_{1.6}O_4$, the *A* (tetrahedral) sites are held to be exclusively occupied by Fe^{2+} and in $Fe_{1.8}Cr_{1.2}O_4$, the *A* sites are believed to be occupied largely by Fe^{2+} with a much smaller occupancy by Fe^{3+} (*11*). It is only in the octahedral *B* sites, occupied by Cr^{3+} and Fe^{3+} in $Fe_{1.4}Cr_{1.6}O_4$ and occupied by Cr^{3+}, Fe^{3+}, and a small amount of Fe^{2+} in $Fe_{1.8}Cr_{1.2}O_4$, that ordering of Cr and Fe cations can occur. For $FeCr_2O_4$, in contrast, the *B* sites are occupied only by Cr^{3+} and the *A* sites only by Fe^{2+}, precluding the ordering of cations at either of the sites.

The bands observed at higher wavenumbers in $FeCr_2O_4$ and $Fe_{1.4}Cr_{1.6}O_4$ can be assigned as overtones or combinations of the fundamental vibrations. The 1357 cm^{-1} band of $FeCr_2O_4$ and the 1335 cm^{-1} band of $Fe_{1.4}Cr_{1.6}O_4$ occur at approximately 2×675 cm^{-1} and are thus overtones of the ~675 cm^{-1} mode. This overtone, with $(A_{1g})^2$ symmetry, is allowed even at the most restrictive point in the Brillouin zone, i.e., the zone center ($k = 0$) (*15*). By analogy to Fe_3O_4, $FeCr_2O_4$ should have a T_{2g} phonon at ~550 cm^{-1} even though it was not observed in the polycrystalline sample. The 1265 cm^{-1} band of $FeCr_2O_4$ can then be assigned as 550 + 686 cm^{-1}, with the $T_{2g} \times A_{1g}$ combination allowed even at the zone center.

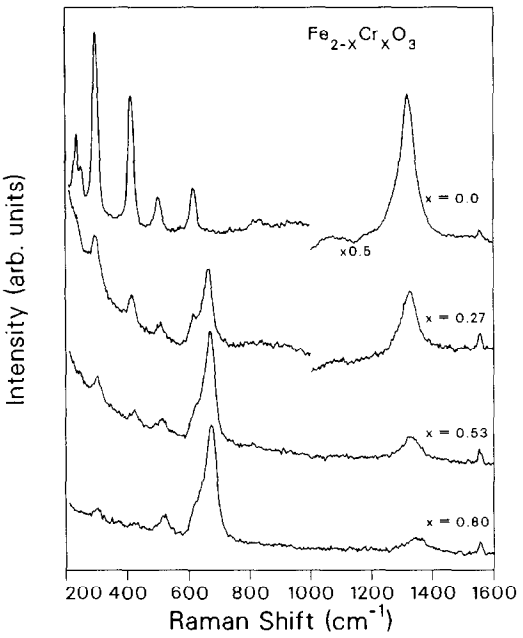

FIG. 2. Raman spectra of corundum-structure solid solution: $Fe_{2-x}Cr_xO_3$ with $x = 0.0, 0.27, 0.53$, and 0.80 using a 514.5-nm laser. Materials containing both Fe and Cr exhibit a new peak at ~675 cm^{-1}. Scale factors are shown.

Results: $Fe_{2-x}Cr_xO_3$ Solid Solutions

The Raman spectra of the corundum-type solid solutions $Fe_{2-x}Cr_xO_3$ with $x = 0.0, 0.27, 0.53, 0.80$ and with $x = 1.07, 1.33, 1.60, 2.0$ are shown in Figs. 2 and 3, respectively. When chromium is substituted for iron in α-Fe_2O_3 (upper spectrum of Fig. 2), a new band appears. The band ranges in Raman shift from 664 cm^{-1} for $Fe_{1.73}Cr_{0.27}O_3$ to 685 cm^{-1} for $Fe_{0.40}Cr_{1.60}O_3$, with

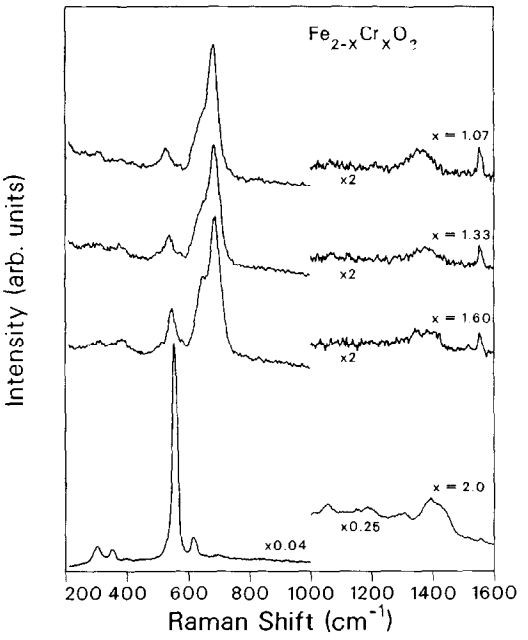

FIG. 3. Raman spectra of corundum-structure solid solution: $Fe_{2-x}Cr_xO_3$ with x = 1.07, 1.33, 1.60, and 2.0 using a 514.5-nm laser. All materials show a peak at ~1350 cm^{-1}. Scale factors are shown.

the shift increasing nearly linearly with increasing chromium content. This new feature was also observed in an earlier, unpublished study of $Fe_{2-x}Cr_xO_3$ solid solutions (*16*). In order to investigate whether the ~675 cm^{-1} feature resulted from sample inhomogeneity, a $Fe_{1.73}Cr_{0.27}O_3$ phase was further annealed for 8 hr at 1300°C in air, followed by an air quench. (Inadequate annealing in the $Fe_{2-x}Cr_xO_3$ system can produce anomalous Mössbauer line shapes, which are believed to result from clusters of one type of cation (*17*).) The Raman spectrum of this sample was nearly identical to that obtained from the original $Fe_{1.73}Cr_{0.27}O_3$ material annealed at only 1200°C.

Table II also contains the lengths of the hexagonal unit cells of $Fe_{2-x}Cr_xO_3$ as determined by X-ray powder diffraction. The cell lengths are in good agreement with literature results (*18*). In the (room temperature) XRD spectra, there was no evidence of superlattice reflections. Nor was there any evidence that the unit cells were distorted away from full rhombohedral symmetry. The $Fe_{2-x}Cr_xO_3$ materials were single phase with no contamination by Fe_{3-x}

TABLE II

OBSERVED RAMAN BANDS AND LATTICE PARAMETERS FOR $Fe_{2-x}Cr_xO_3$

α-Fe_2O_3	236	253	298	413	502	616	—	1319 + weak peaks at 831 and 1073
a = 5.037 (1), c = 13.752 (3)								
$Fe_{1.73}Cr_{0.27}O_3$	—	—	298	417	508	616	664	1328 + weak peak at 1073
a = 5.032 (1), c = 13.710 (3)								
$Fe_{1.47}Cr_{0.53}O_3$	—	—	305	423	515	625	670	1329
a = 5.025 (1), c = 13.676 (3)								
$Fe_{1.20}Cr_{0.80}O_3$	—	—	303	424	521	620	673	1343
a = 5.017 (1), c = 13.650 (3)								
$Fe_{0.93}Cr_{1.07}O_3$	—	—	310	382	527	639	682	1359
a = 5.008 (1), c = 13.631 (3)								
$Fe_{0.67}Cr_{1.33}O_3$	—	—	—	386	537	648	683	1370
a = 4.996 (1), c = 13.622 (3)								
$Fe_{0.40}Cr_{1.60}O_3$	—	—	310	385	547	648	685	1381
a = 4.981 (1), c = 13.608 (3)								
Cr_2O_3	—	304	353	529	553	616	—	1398 + weak peaks at 401, 698, 1056,
a = 4.961 (1), c = 13.599 (2)								1154, 1210, and 1300

Note. All Raman shift values are in cm^{-1}. Rhombohedral lattice parameters are expressed as hexagonal unit cells with a and c in Å, with error of last digit in parentheses.

Cr_xO_4. Thus the ~675 cm^{-1} band of $Fe_{2-x}Cr_xO_3$ cannot be due to $Fe_{3-x}Cr_xO_4$ impurities.

Several of the bands of α-Fe_2O_3 are relatively unaltered by the substitution of chromium for iron. For example, the 298, 413, 502, and 616 cm^{-1} bands of α-Fe_2O_3 can be seen at progressively higher Raman shifts for chromium additions up to $Fe_{1.20}Cr_{0.80}O_3$. The evolution of one phonon, the 502 cm^{-1} band of α-Fe_2O_3, can be followed through the entire range of solid solution. The Raman shift increases nearly linearly with increasing chromium content. The change toward higher frequency with increasing chromium content results from the contraction of the unit cell. A Grüneisen constant of 2.4 is found for this mode.

Discussion: $Fe_{2-x}Cr_xO_3$ Solid Solutions

Seven Raman-active fundamental vibrations are predicted by group-theoretical analysis of the $R\bar{3}c$ (D_{3d}^6) crystal structure (*19*). All these modes have been observed in single-crystal studies of α-Fe_2O_3 (*20, 21*) and Cr_2O_3 (*21, 22*). The upper spectrum of Fig. 2 gives the Raman spectrum of α-Fe_2O_3. Following the results of Hart *et al.* (*20*), the fundamental vibrations and symmetries can be assigned as follows: 236 cm^{-1} (A_{1g}), 253 cm^{-1} (E_g), 298 cm^{-1} (E_g and E_g), 413 cm^{-1} (E_g), 502 cm^{-1} (A_{1g}), and 616 cm^{-1} (E_g). In the room-temperature spectrum of α-Fe_2O_3, the 298 cm^{-1} band is actually two unresolved fundamental vibrations both of E_g symmetry (*21*). The lower spectrum of Fig. 3 gives the spectrum of Cr_2O_3. Following the results of Hart *et al.* (*22*), the fundamental vibrations and symmetries can be assigned as follows: 304 cm^{-1} (E_g), 353 cm^{-1} (E_g), 529 cm^{-1} (E_g), 553 cm^{-1} (A_{1g}), and 616 cm^{-1} (E_g). The two remaining fundamental vibrations (235 cm^{-1} (E_g) and 266 cm^{-1} (A_{1g})) are relatively weak and were not observed here.

Scattering from the magnetic structure of α-Fe_2O_3 and Cr_2O_3 (i.e., magnon scattering), must be considered when analyzing the Raman spectra of $Fe_{2-x}Cr_xO_3$. Hematite, α-Fe_2O_3, is antiferromagnetic below the Morin transition of 260 K and has a slight ferromagnetic moment between 260 K and the Néel temperature of 960 K (*23*). Above 960 K, the spins of the Fe^{3+} ions are disordered and α-Fe_2O_3 is paramagnetic. Cr_2O_3 is antiferromagnetic below its Néel temperature of 311 K (*24*). While no one-magnon features have been observed in α-Fe_2O_3 (*20, 25*), both one- and two magnon scatterings have been identified in Cr_2O_3 (*22*). Although extremely weak at room temperature, the one-magnon scattering was observed here at 401 cm^{-1}. In addition, a broad and weak band at approximately 698 cm^{-1}, previously identified as two-magnon scattering, was detected. The strongest feature in the spectrum of α-Fe_2O_3, at 1319 cm^{-1}, had until recently been assigned as two-magnon scattering (*20, 25*). Figures 2 and 3 show that the entire solid solution $Fe_{2-x}Cr_xO_3$ exhibits a peak in this region (~1350 cm^{-1}) that varies nearly linearly in Raman shift as a function of composition.

The origin of the ~675 and ~1350 cm^{-1} peaks has been recently discussed (*26*) and the results are summarized here. The ~1350 cm^{-1} peaks of the mixed-metal materials occur at almost exactly twice the frequency of the ~675 cm^{-1} peak, clearly establishing that the ~1350 cm^{-1} peaks are overtones of the ~675 cm^{-1} peaks. The temperature dependence of ~675 and ~1350 cm^{-1} peaks establish that they arise from phonon scattering, not magnon scattering. This interpretation is supported by the Grüneisen constants of 1.1 and 1.5 for the ~675 and ~1350 cm^{-1} bands, respectively. These values are typical of normal phonon behavior. Given the relative sharpness of the ~675 cm^{-1} peaks, it is probable that they arise from first-order phonon scattering. Both α-Fe_2O_3 and Cr_2O_3 have IR-

active normal modes at frequencies close to the values extrapolated from the frequency–composition relationship of the solid solutions (*27, 28*). Therefore, it is believed that the ~675 cm^{-1} features are IR-active modes that are Raman inactive in α-Fe_2O_3 and Cr_2O_3 and that these modes become active in the mixed-metal solid solutions as a result of symmetry relaxation processes. This makes the ~1350 cm^{-1} peaks, observed for the entire Fe_2O_3–Cr_2O_3 solid solution, overtones of a fundamental vibrational mode that is observed only for the mixed-metal solid solutions.

The spectrum of Cr_2O_3 contains weak, broad features at approximately 1056, 1154, 1190, and 1300 cm^{-1}. While the symmetries of these features could not be determined from the polycrystalline samples, it is believed that they arise from overtones or combinations of the fundamental vibrations. The 1056 cm^{-1} feature is approximately 2 × 529 cm^{-1} and the overtone of $(E_g)^2$ symmetry is allowed at $k = 0$ by group theory considerations (*15*). The 1154 cm^{-1} feature is approximately 616 + 529 or 616 + 553 and the combinations of $E_g \times E_g$ or $E_g \times A_{1g}$ symmetry are both Raman allowed at $k = 0$. The 1210 cm^{-1} feature is approximately 2 × 616 cm^{-1} and the $(E_g)^2$ symmetry is again allowed. It is not possible to assign the weak 1300 cm^{-1} feature on a similar basis.

Comparison of $Fe_{3-x}Cr_xO_4$ and $Fe_{2-x}Cr_xO_3$

For the $Fe_{2-x}Cr_xO_3$ solid solution, both the ~525 and ~1350 cm^{-1} peaks vary as nearly linear functions of composition and thus compositions can be unambiguously determined by Raman scattering (Table II). For the $Fe_{3-x}Cr_xO_4$ solid solution, the situation is not so straightforward. While the Raman shift of the dominant peak (~675 cm^{-1}) changes with composition, the change is not a monotonic function of composition (Table I). However, by careful examination of the frequency and FWHM of the ~675 cm^{-1} peak, the relative intensity of the ~550 cm^{-1} peak, and whether there are shoulders at ~635 cm^{-1}, it is possible to estimate composition from the Raman spectra.

In studies of Fe–Cr alloy oxidation, Raman spectroscopy has been used to identify the different Fe–Cr oxides. However, care must be exercised when using Raman spectroscopy to distinguish between $Fe_{2-x}Cr_xO_3$ and $Fe_{3-x}Cr_xO_4$ solid solutions since the most intense feature of both solid solutions occurs at ~675 cm^{-1}. $Fe_{3-x}Cr_xO_4$ with x less than ~0.8 and $x \approx 2$ can clearly be distinguished from all $Fe_{2-x}Cr_xO_3$ phases since these $Fe_{3-x}Cr_xO_4$ phase have an isolated peak at ~675 cm^{-1}, while for the $Fe_{2-x}Cr_xO_3$ phase the ~675 cm^{-1} peak is merged with a peak at ~640 cm^{-1}. However, $Fe_{1.8}Cr_{1.2}O_4$ and $Fe_{1.4}Cr_{1.6}O_4$ have shoulders on the low wavenumber side of the ~675 cm^{-1} peaks. These phases can be distinguished from $Fe_{2-x}Cr_xO_3$ by examining the ~550 cm^{-1} peaks of $Fe_{3-x}Cr_xO_4$. In $Fe_{1.8}Cr_{1.2}O_4$ and $Fe_{1.4}Cr_{1.6}O_4$, this peak is extremely broad. In $Fe_{2-x}Cr_xO_3$, peaks occur in this region only for high chromium-content materials with the peaks being quite sharp compared to $Fe_{1.8}Cr_{1.2}O_4$ and $Fe_{1.4}Cr_{1.6}O_4$. Reports in the literature have inferred the presence of $Fe_{3-x}Cr_xO_4$ from materials with peaks at ~675 cm^{-1} (*29, 30*). In some instances, however, the spectra exhibit a much closer agreement with those of $Fe_{2-x}Cr_xO_3$. That is, the spectra contain peaks at both ~640 and ~680 cm^{-1}, a feature indicative of $Fe_{2-x}Cr_xO_3$, not $Fe_{3-x}Cr_xO_4$.

Acknowledgment

The authors thank D. Dominguez for assistance in preparing the samples.

References

1. H. J. Levinstein, M. Robbins, and C. Capio, *Mater. Res. Bull.* **7**, 27 (1972).

2. D. E. Cox, W. J. Takei, and G. Shirane, *J. Phys. Chem. Solids* **24,** 405 (1963).
3. J. C. Hamilton, B. E. Mills, and R. E. Benner, *Appl. Phys. Lett.* **40,** 499 (1982).
4. F. S. Galasso, "Structure and Properties of Inorganic Solids," Chaps. 8 and 9, Pergamon, Oxford (1970).
5. T. Katsura and A. Muan, *Trans. Metall. Soc. AIME* **230,** 77 (1964).
6. G. Herzberg, "Molecular Spectra and Molecular Structure," Vol. 1, p. 62, Van Nostrand–Reinhold, New York (1950).
7. W. D. Derbyshire and H. J. Yearian, *Phys. Rev.* **112,** 1603 (1958).
8. T. R. Hart, H. Temkin, and S. B. Adams, "Proceedings of the Third International Conference on Light Scattering in Solids" (M. Balkanski, R. C. C. Leite, and S. P. S. Porto, Eds.), p. 254, Wiley, New York (1975).
9. C. Kittel, "Introduction to Solid State Physics," 3rd ed., p. 184, Wiley, New York (1953).
10. J. L. Verble, *Phys. Rev. B* **9,** 5236 (1974).
11. M. Robbins, G. K. Wertheim, R. C. Sherwood, and D. N. E. Buchanan, *J. Phys. Chem. Solids* **32,** 717 (1971).
12. B. Gillot, F. Bouton, J. F. Ferriot, F. Chassagneux, and A. Rousset, *J. Solid State Chem.* **21,** 375 (1977).
13. B. A. DeAngelis, V. G. Keramidas, and W. B. White, *J. Solid State Chem.* **3,** 358 (1971).
14. V. G. Keramidas, B. A. DeAngelis, and W. B. White, *J. Solid State Chem.* **15,** 233 (1975).
15. J. C. Decius and R. M. Hexter, "Molecular Vibrations in Crystals," Chap. 4, McGraw–Hill, New York (1977).
16. R. E. Benner, J. C. Hamilton, A. S. Nagelberg, and P. L. Mattern, Sandia National Laboratories Report SAND81-8820, p. 25 (1982).
17. J. K. Srivastava and R. P. Sharma, *J. Phys. Coll. Suppl.* **6,** 663 (1974).
18. P. E. Wretblad, *Z. Anorg. Allg. Chem.* **189,** 329 (1930).
19. S. Bhagavantam and T. Venkatarayudu, *Proc. Indian Acad. Sci. A* **9,** 224 (1939).
20. T. R. Hart, S. B. Adams, and H. Temkin, "Proceedings of the Third International Conference on Light Scattering in Solids" (M. Balkanski, R. C. C. Leite, and S. P. S. Porto, Eds.), p. 259, Wiley, New York (1976).
21. I. R. Beattie and T. R. Gilson, *J. Chem. Soc. A* **5,** 980 (1970).
22. T. R. Hart, R. L. Aggarwal, and B. Lax, "Proceedings of the Second International Conference on Light Scattering in Solids" (M. Balkanski, Ed.), p. 174, Flammarion Sciences, Paris (1971).
23. F. J. Morin, *Phys. Rev.* **78,** 819 (1950).
24. E. P. Trounson, D. F. Bleil, R. K. Wangsness, and L. R. Maxwell, *Phys. Rev.* **79,** 542 (1950).
25. T. P. Martin, R. Merlin, D. R. Huffman, and M. Cardona, *Solid State Commun.* **22,** 565 (1977).
26. K. F. McCarty, *Solid State Commun.* **68,** 799 (1988).
27. S. Onari, T. Arai, and K. Kudo, *Phys. Rev. B* **16,** 1717 (1977).
28. G. Lucovsky, R. J. Sladek, and J. W. Allen, *Phys. Rev. B* **16,** 4716 (1977).
29. S. C. Tjong, *Mater. Res. Bull.* **18,** 157 (1983).
30. D. J. Gardiner, C. J. Littleton, K. M. Thomas, and K. N. Strafford, *Oxid. Met.* **27,** 57 (1987).